AARHUS UNIVERSITY

Wind Energy

Final Project

Wake-flow Simulation of Wind Farms

Individual Report

Mohammad Khalikujjaman

AU ID: 785559

Department of Mechanical and Production Engineering
Aarhus University

Submission date: 19 May 2026

Contents

1 Introduction and Project Objective

Wind-farm performance is strongly affected by wake interaction between turbines. When an upstream turbine extracts momentum from the incoming atmospheric boundary layer, it creates a region of reduced mean velocity and increased turbulence intensity. A downstream turbine operating inside this wake receives a lower effective wind speed and a modified turbulence environment, which directly affects power production and wake loading. For this reason, wake prediction is an important part of wind-farm layout assessment.

The objective of this final project is to simulate wake flow in three six-turbine wind-farm layouts using OpenFOAM and to evaluate the realizable k–ε RANS model against the provided LES reference data. The project is divided into three main tasks. Task 1 concerns the construction of the OpenFOAM cases for the three layouts. Task 2 concerns simulation, post-processing, and comparison with LES. Task 3 concerns the interpretation of how the changes in layout affect wake behaviour and how the RANS model performs under different wake-interaction regimes.

The three layouts are shown in Figure 1. Case A is the reference aligned layout with $7d_0$ streamwise spacing. Case B is also aligned, but the spacing is reduced to $5d_0$. Case C keeps the $7d_0$ streamwise spacing but shifts the even turbine rows laterally by one rotor diameter. The comparison is made using rotor-averaged velocity deficit, rotor-averaged turbulence intensity, hub-height contour fields, and normalized turbine-row power.

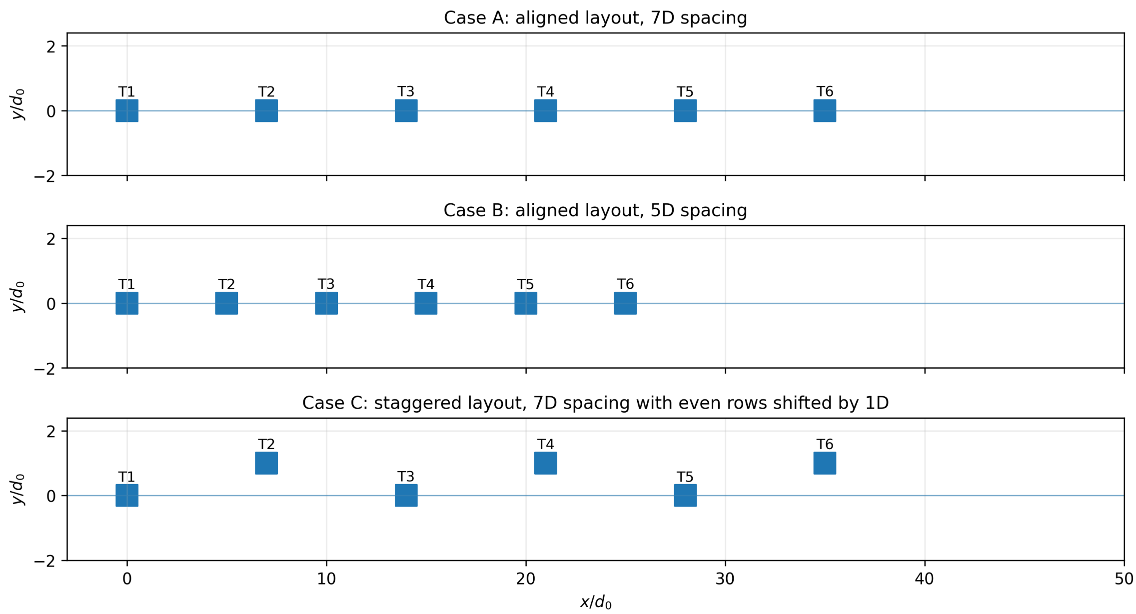

Figure 1: Schematic representation of the three wind-farm layouts. Case A is the aligned $7d_0$ layout, Case B is the aligned $5d_0$ layout, and Case C is the staggered $7d_0$ layout where the even turbine rows are shifted by d_0 in the lateral direction.

2 Task 1: OpenFOAM Case Construction

2.1 Base numerical setup

The simulations are based on the Mini Project 2 realizable k–ε OpenFOAM case. The wind farm consists of six turbines with rotor diameter $d_0 = 80$ m, hub height $z_h = 70$ m, and axial induction factor $a = 0.25$. The hub-height inflow velocity is $u_h = 8\ \mathrm{m\,s^{-1}}$, and the hub-height turbulence intensity is $I_{k,h} = 5.8\%$.

The computational domain has dimensions 4400 m × 400 m × 355 m in the x, y, and z directions. The mesh resolution is 234 × 40 × 58. The first turbine is located at $x/d_0 = 0$, while the inlet is located at $x/d_0 = -5$. The same atmospheric boundary-layer inflow, side cyclic boundaries, pressure outlet, rough-wall bottom condition, and top boundary settings were used for all three cases. The turbine forces were applied using actuator-disk source terms in `fvOptions`, with disk regions selected using `topoSetDict`.

2.2 Layout-specific case setup

Table 1 summarizes the turbine locations. Case A was created by extending the Mini Project 2 case from one actuator disk to six actuator disks. The `topoSetDict` and `fvOptions` files were modified to define six disk regions and six actuator-disk force terms. The `blockMeshDict` was kept from the base wind-farm mesh because the streamwise refinement already corresponded to the $7d_0$ turbine spacing.

For Case B, the turbine positions were changed to the aligned $5d_0$ layout. Therefore, `topoSetDict` and `fvOptions` were modified to place the disks at $x/d_0 = 0, 5, 10, 15, 20, 25$. In addition, `blockMeshDict` was changed so that the streamwise mesh refinement remained aligned with the new turbine positions. This was necessary because the refinement zones from Case A would not correctly cover the turbine positions in the shorter-spacing layout.

For Case C, the streamwise positions are the same as in Case A, so the `blockMeshDict` was kept unchanged. However, the even turbine rows were moved laterally by d_0. Therefore, `topoSetDict` and `fvOptions` were modified to shift turbine rows 2, 4, and 6 in the y direction.

Table 1: Turbine centre locations used for the three OpenFOAM cases. Coordinates are normalized by d_0.

Case	Layout	x/d_0 positions	y/d_0 positions
A	$7d_0$ aligned	0, 7, 14, 21, 28, 35	0, 0, 0, 0, 0, 0
B	$5d_0$ aligned	0, 5, 10, 15, 20, 25	0, 0, 0, 0, 0, 0
C	$7d_0$ staggered	0, 7, 14, 21, 28, 35	0, 1, 0, 1, 0, 1

2.3 Run procedure and convergence

Each case was run using the same OpenFOAM workflow: `blockMesh`, `checkMesh`, `topoSet`, `decomposePar`, parallel `simpleFoam`, `reconstructPar`, `linesample`, `writeCellCentres`, and `writeCellVolumes`. The final-time `C` and `V` files were generated for post-processing.

All three simulations converged successfully. The mesh checks did not report failed, severe, or error messages. The convergence summary is given in Table 2. This confirms that the three OpenFOAM folders were constructed correctly and were suitable for the LES comparison in Task 2.

Table 2: Simulation convergence and mesh-check summary.

Case	Layout	SIMPLE iterations	Status
Case A	$7d_0$ aligned	424	Converged, mesh check passed
Case B	$5d_0$ aligned	431	Converged, mesh check passed
Case C	$7d_0$ staggered	433	Converged, mesh check passed

3 Post-processing Method

The comparison with LES was made using four outputs: rotor-averaged velocity deficit, rotor-averaged turbulence intensity, normalized turbine-row power, and hub-height contour fields.

The normalized velocity deficit was calculated as

$$\frac{\Delta u}{u_h} = \frac{u_{in} - u}{u_h}, \tag{1}$$

where u_h is the hub-height inflow velocity and u is the local streamwise velocity. Rotor averaging was performed over the circular rotor area on each x-normal plane using the local cell volumes. For Cases A and B, the averaging line followed the aligned turbine centreline. For Case C, it followed the odd turbine row line, as required by the project instructions.

The turbulence intensity was calculated from the turbulent kinetic energy field as

$$I = \frac{\sqrt{2k/3}}{u_h} \times 100. \tag{2}$$

The same rotor-averaging procedure was then applied to I.

For the power comparison, the final power value from each actuator-disk folder was extracted from the last line of the corresponding `ADM_NR_diskBased.dat` file. The normalized row power was then calculated as

$$\frac{P_i}{P_1}, \tag{3}$$

where P_i is the power of turbine row i and P_1 is the first-row power.

For the contour comparison, the hub-height velocity-deficit and turbulence-intensity fields were extracted from the final OpenFOAM solution. The RANS contours were compared with the LES contour figures provided in the tutorial appendix. The same visual scale was kept as closely as possible: approximately $0 \leq \Delta u/u_h \leq 0.8$ for velocity deficit and $4\% \leq I \leq 16\%$ for turbulence intensity. This makes the LES and RANS contour fields directly comparable.

The following error measures were also calculated:

$$\mathrm{MAE} = \frac{1}{N}\sum_{i=1}^{N} \left| q_i^{\mathrm{RANS}} - q_i^{\mathrm{LES}} \right|, \tag{4}$$

$$\mathrm{RMSE} = \left[\frac{1}{N}\sum_{i=1}^{N} \left(q_i^{\mathrm{RANS}} - q_i^{\mathrm{LES}} \right)^2 \right]^{1/2}. \tag{5}$$

For turbulence intensity, these errors are reported in percentage points.

4 Task 2: Simulation Results and Comparison with LES

4.1 Rotor-averaged velocity deficit

Figure 2 compares the rotor-averaged velocity deficit for the three cases. In all cases, the RANS model captures the general decay of the wake deficit downstream. However, the model tends to predict a weaker deficit than LES in the aligned layouts. This means that the wake recovers too quickly in the RANS simulation, especially before the second turbine row.

In Case A, the overall trend is captured, but the early downstream wake is weaker in RANS than in LES. In Case B, the shorter $5d_0$ spacing makes this issue more important because the next turbine is placed before the wake has enough distance to recover. In Case C, the rotor-averaged deficit error is slightly lower, partly because the staggered layout reduces direct wake overlap along the odd turbine line.

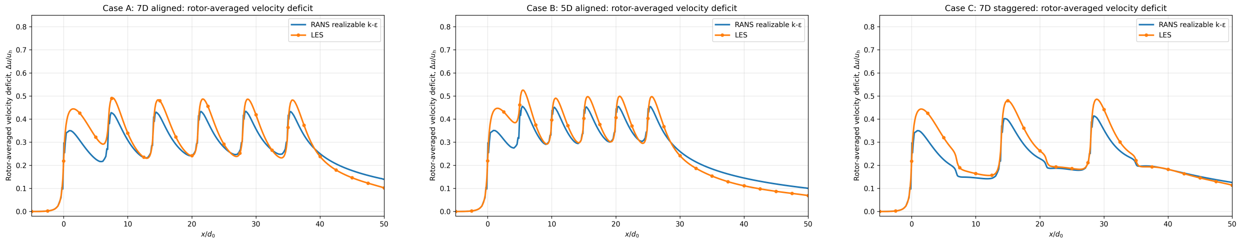

(a) Case A **(b)** Case B **(c)** Case C

Figure 2: Rotor-averaged normalized velocity deficit for Cases A–C. Each panel compares the realizable k–ε RANS result with the corresponding LES reference data.

4.2 Rotor-averaged turbulence intensity

Figure 3 shows the rotor-averaged turbulence intensity. The RANS model gives a reasonable prediction of the general turbulence level and its downstream development. The agreement is best in Case C and slightly weaker in Case B. This is expected because the shorter spacing in Case B gives stronger wake interaction and sharper turbulence variations, while the staggered arrangement in Case C reduces direct wake overlap.

The RANS curves are smoother than the LES data. This is reasonable because LES resolves more unsteady turbulent structures, while the steady RANS model represents turbulence through averaged quantities and an eddy-viscosity closure.

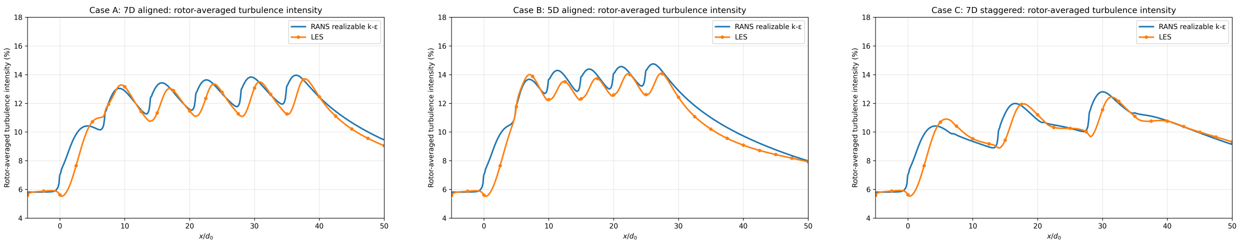

(a) Case A **(b)** Case B **(c)** Case C

Figure 3: Rotor-averaged turbulence intensity for Cases A–C. The RANS model captures the general turbulence level, but the LES data show more detailed spatial variation.

4.3 Normalized turbine-row power

Figure 4 and Table 3 compare the normalized turbine-row power. This is an important engineering quantity because even moderate velocity errors can lead to noticeable power differences.

For Case A, the RANS model predicts $P_2/P_1 = 0.5708$, while LES gives 0.4204. This indicates that RANS underestimates the wake loss at the second turbine row. For Case B, the same problem is stronger: RANS predicts 0.4745 for row 2, while LES gives 0.2742. This shows that the closely spaced aligned case is the most difficult for the model. In Case C, the agreement for row 2 is very good: RANS gives 0.9614 and LES gives 0.9581. This shows that the model captures the main benefit of shifting the even rows laterally.

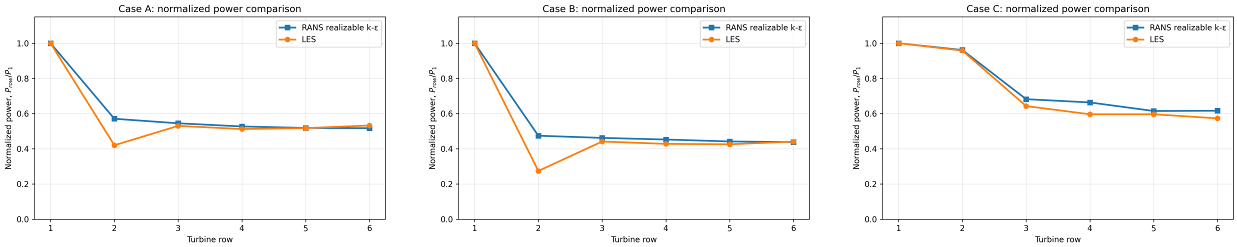

(a) Case A **(b)** Case B **(c)** Case C

Figure 4: Normalized turbine-row power for Cases A–C. The power of each row is normalized by the first-row power.

Table 3: Normalized turbine-row power comparison between RANS and LES. The difference is calculated as RANS minus LES.

Case	Row	RANS P_i/P_1	LES P_i/P_1	Difference
A	1	1.0000	1.0000	0.0000
A	2	0.5708	0.4204	0.1504
A	3	0.5451	0.5302	0.0149
A	4	0.5270	0.5124	0.0146
A	5	0.5188	0.5177	0.0011
A	6	0.5173	0.5327	-0.0154
B	1	1.0000	1.0000	0.0000
B	2	0.4745	0.2742	0.2003
B	3	0.4620	0.4414	0.0206
B	4	0.4528	0.4281	0.0247
B	5	0.4418	0.4258	0.0160
B	6	0.4383	0.4409	-0.0026
C	1	1.0000	1.0000	0.0000
C	2	0.9614	0.9581	0.0033
C	3	0.6821	0.6429	0.0392
C	4	0.6636	0.5963	0.0673
C	5	0.6149	0.5963	0.0186
C	6	0.6164	0.5732	0.0432

4.4 Hub-height contour comparison

Figures 5–10 compare the LES and RANS hub-height contour fields. In each figure, panel (a) is the LES reference from the tutorial appendix, and panel (b) is the present realizable k–ε RANS result. The same approximate colour ranges are used so that wake width, wake strength, and turbulence distribution can be compared directly.

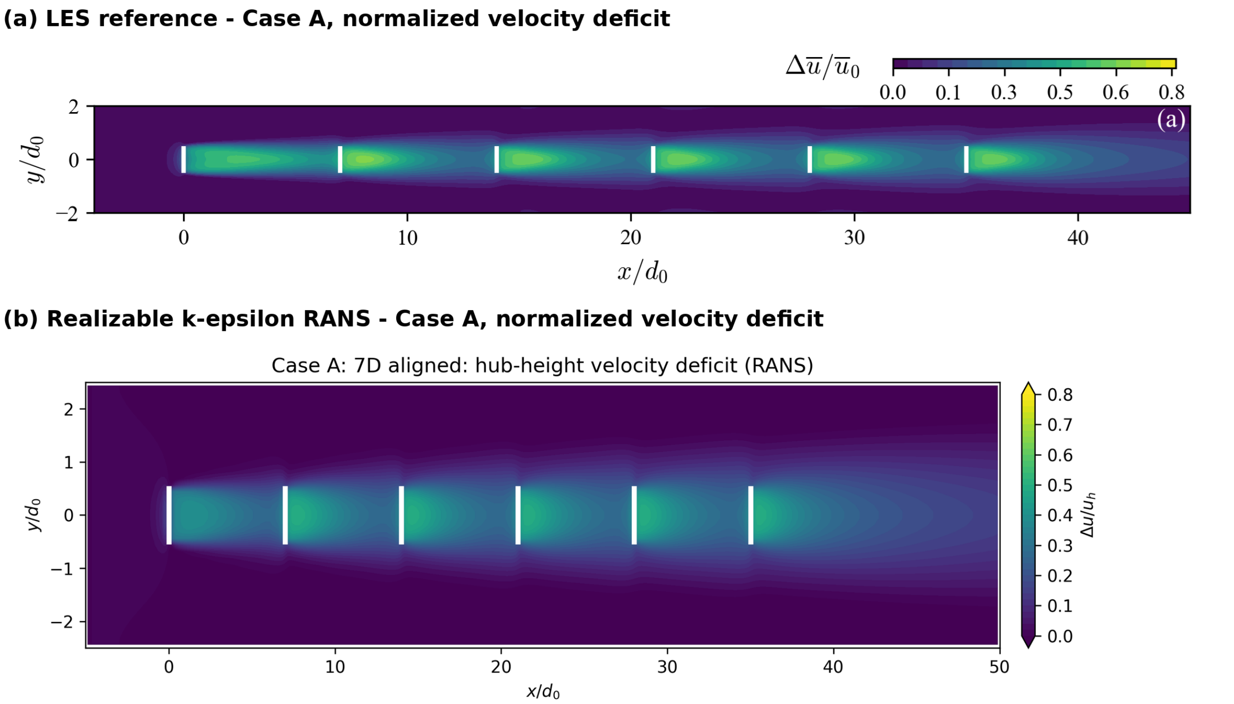

Figure 5: Hub-height normalized velocity-deficit contours for Case A. The RANS result captures the aligned wake corridor, but the wake is broader and smoother than in the LES reference.

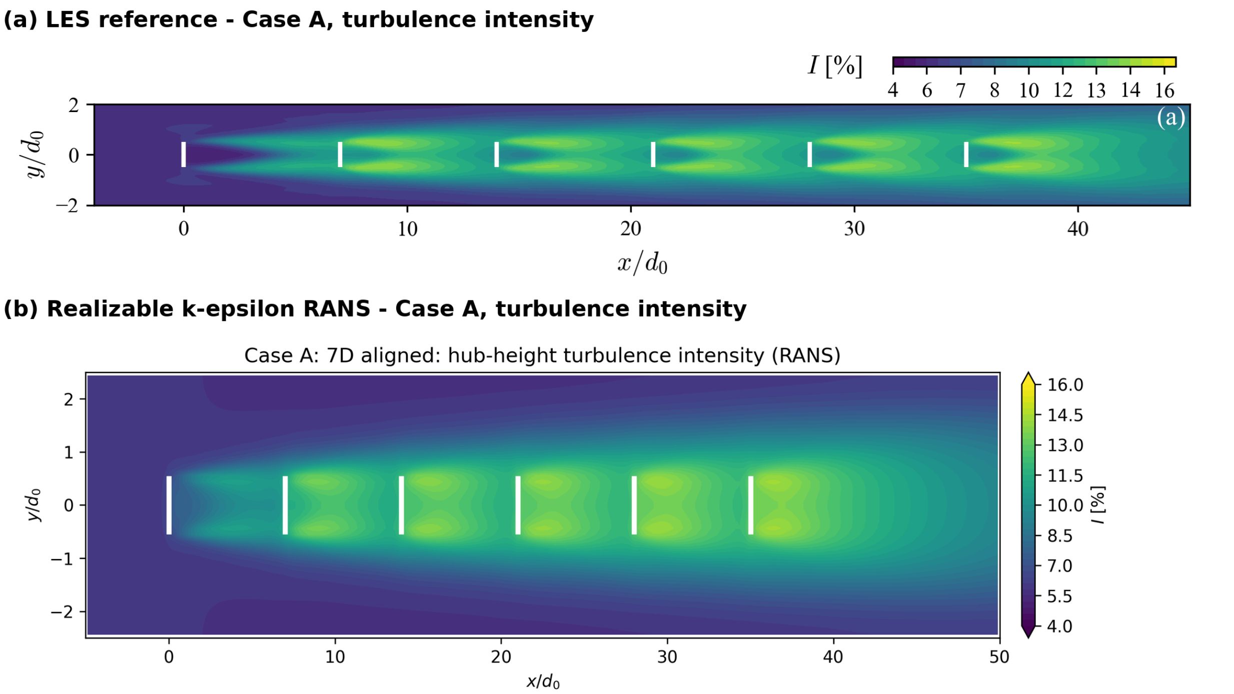

Figure 6: Hub-height turbulence-intensity contours for Case A. The RANS result reproduces the broad turbulent wake region but smooths the smaller spatial structures visible in LES.

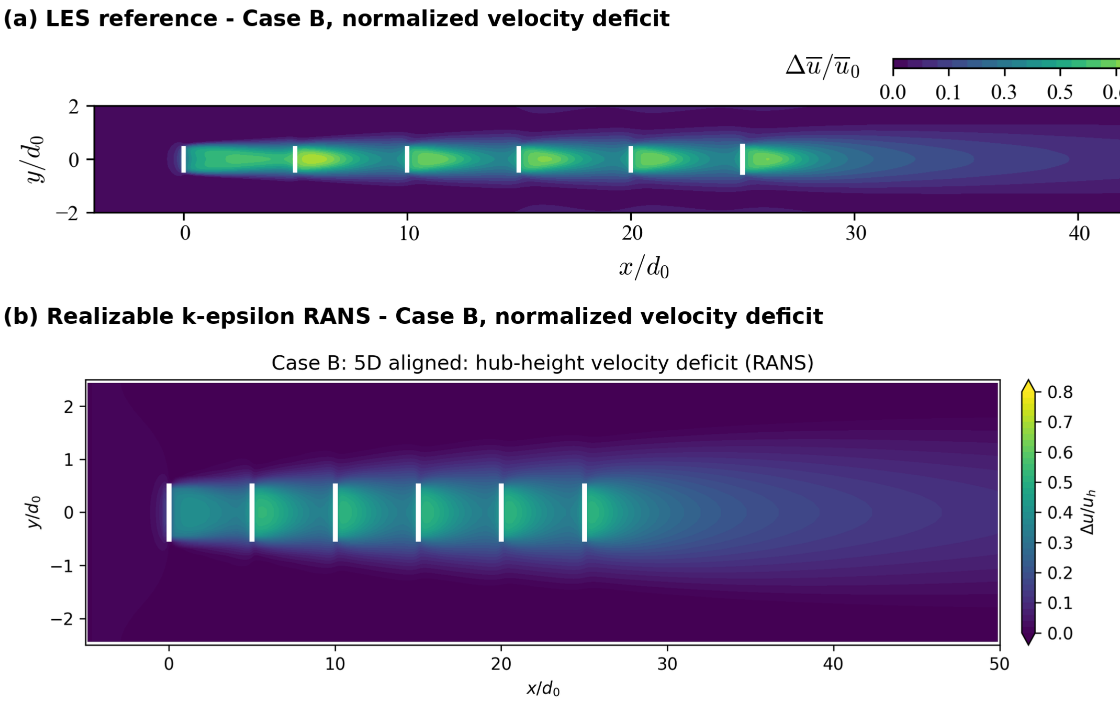

Figure 7: Hub-height normalized velocity-deficit contours for Case B. The shorter $5d_0$ spacing creates stronger interaction between turbine wakes and gives less distance for recovery.

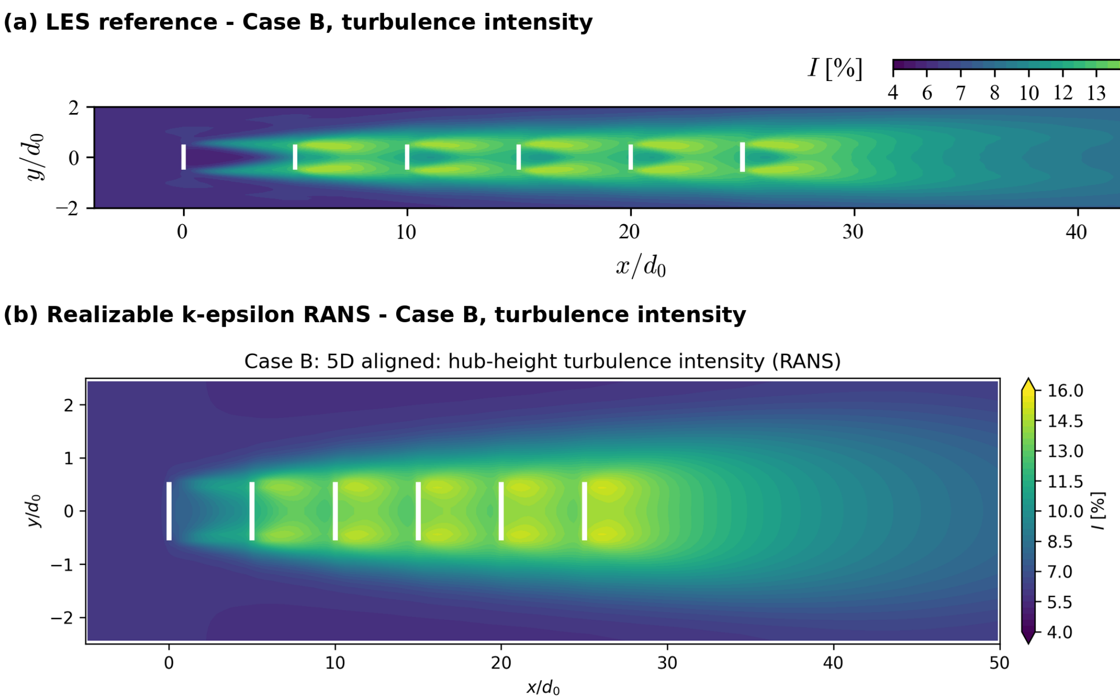

Figure 8: Hub-height turbulence-intensity contours for Case B. RANS predicts a smooth high-turbulence corridor, while LES shows more detailed wake structures.

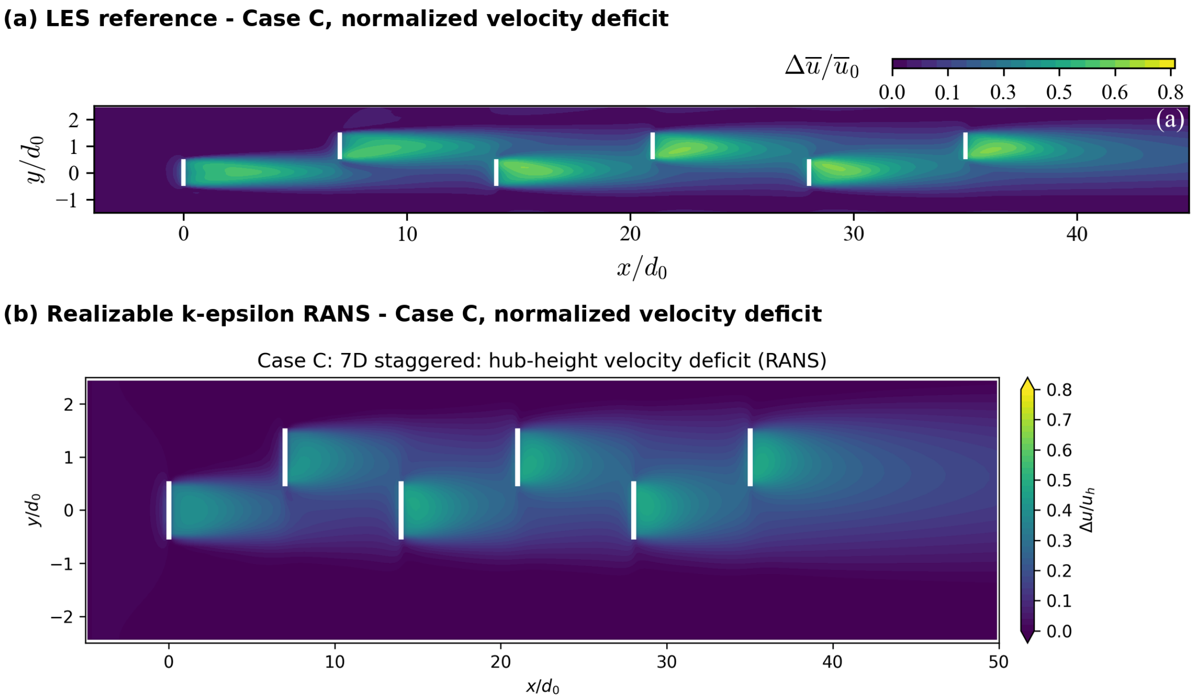

Figure 9: Hub-height normalized velocity-deficit contours for Case C. The staggered arrangement shifts the even rows away from the strongest upstream wake region and spreads the wake laterally.

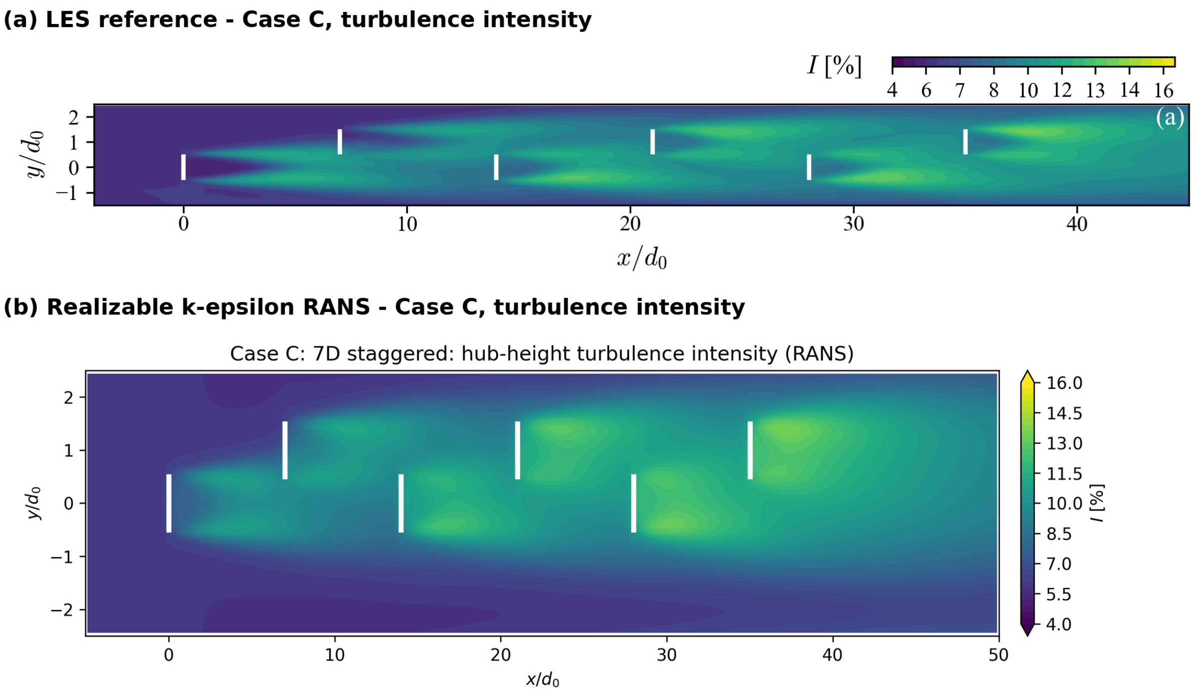

Figure 10: Hub-height turbulence-intensity contours for Case C. The lateral shift produces a more three-dimensional wake pattern, while the RANS field remains smoother than the LES reference.

4.5 Error summary

Table 4 summarizes the quantitative errors. The velocity-deficit errors are similar for the three cases. The turbulence-intensity error is lowest in Case C. The power error shows the clearest layout dependence: Case B has the largest power RMSE, while Case C has the smallest. This supports the observation that the model performs best when direct wake overlap is reduced and struggles more in the dense aligned case.

Table 4: Quantitative comparison between RANS and LES. Turbulence-intensity errors are reported in percentage points.

Case	Deficit MAE	Deficit RMSE	TI MAE	TI RMSE	Power MAE	Power RMSE
A	0.0352	0.0463	0.6751	0.9997	0.0327	0.0623
B	0.0334	0.0430	0.6910	0.9314	0.0440	0.0831
C	0.0312	0.0463	0.5004	0.8278	0.0286	0.0372

5 Task 3: Discussion of Layout Effects and RANS Performance

5.1 Case A to Case B: effect of reducing spacing

The main change from Case A to Case B is the reduction of the streamwise spacing from $7d_0$ to $5d_0$. This gives the wake less distance to recover before it reaches the next turbine row. Therefore, stronger wake interaction and lower downstream power are expected in Case B.

The LES data confirm this clearly. The second-row normalized power decreases from 0.4204 in Case A to 0.2742 in Case B. The RANS model captures the same qualitative trend because its second-row power also decreases from Case A to Case B. However, the model still overpredicts the second-row power in both aligned cases. This means that the realizable k–ε model predicts too much wake recovery before the second row, especially in the closely spaced aligned layout.

For engineering use, this is an important limitation. If the RANS result is used alone, a dense aligned layout may appear more productive than it would be according to LES. Therefore, Case B shows that steady eddy-viscosity RANS should be used carefully for strong multi-row wake interaction.

5.2 Case A to Case C: effect of lateral staggering

The main change from Case A to Case C is the lateral shift of the even turbine rows by d_0. This means that the second row is no longer placed directly in the centre of the strongest wake from the first row. As a result, the second row receives a much higher effective inflow velocity.

This is visible in the power comparison. The second-row LES power increases from 0.4204 in Case A to 0.9581 in Case C. The RANS model predicts this improvement very well, with $P_2/P_1 = 0.9614$ in Case C. This shows that the model captures the main physical benefit of staggering: reduced direct wake overlap.

Further downstream, the staggered layout gives a more complex wake pattern because the wake is spread laterally. RANS still smooths the detailed turbulent structures compared with LES, but it predicts the overall redistribution of the wake reasonably well. This is why Case C gives the lowest power error among the three cases.

5.3 Overall RANS model performance

The realizable k–ε model gives useful mean-flow predictions, especially for identifying the relative effect of different wind-farm layouts. It correctly predicts that Case B is the most wake-affected layout and that Case C benefits from lateral staggering. However, it also shows a clear limitation: it tends to recover the wake too quickly in the aligned cases.

This limitation is connected to the modelling approach. The actuator-disk model applies a distributed momentum sink but does not resolve rotating blades, tip vortices, root vortices, or detailed near-wake structures. In addition, RANS gives a time-averaged flow field and cannot directly resolve unsteady wake meandering. The eddy-viscosity turbulence model also smooths velocity and turbulence gradients. These effects can lead to excessive mixing and faster wake recovery than in LES.

The connection between turbulence intensity and wake recovery is important. Higher turbulence generally increases mixing between the wake and the surrounding higher-momentum flow. This can accelerate velocity recovery, but it can also affect downstream turbine loading. In the present results, the RANS turbulence fields are smoother than the LES fields. This helps explain why RANS predicts smoother wake recovery and why the power in the aligned downstream rows is overestimated.

6 Conclusion

Three wind-farm layouts were constructed and simulated in OpenFOAM using the realizable k–ε RANS model. Case A was an aligned $7d_0$ layout, Case B was an aligned $5d_0$ layout, and Case C was a staggered $7d_0$ layout with even rows shifted laterally by one rotor diameter. All three simulations converged successfully, and the final results were compared with LES using rotor-averaged wake quantities, hub-height contours, and normalized turbine-row power.

The results show that the RANS model captures the main qualitative layout effects. Reducing the spacing from $7d_0$ to $5d_0$ increases wake interaction and decreases downstream power. Shifting the even rows laterally reduces direct wake overlap and strongly improves the second-row power. The model performs best for Case C, where the power RMSE is 0.0372, and worst for Case B, where the power RMSE is 0.0831.

The main limitation is the overprediction of wake recovery in the aligned cases. This is most visible at the second turbine row. In Case A, RANS predicts $P_2/P_1 = 0.5708$ while LES gives 0.4204. In Case B, RANS predicts 0.4745 while LES gives 0.2742. This shows that the RANS/actuator-disk setup underestimates the severity of the first wake before it reaches the second turbine row.

Overall, the study shows that wind-farm layout has a strong effect on wake characteristics and power production. The realizable k–ε model is useful for identifying broad layout trends, but higher-fidelity modelling such as LES is still important when accurate quantitative prediction is needed for dense aligned wind-farm layouts.

References

[1] N. Zehtabiyan-Rezaie, *Wake-flow Simulation of Wind Farms: Final Project Tutorial*, Wind Energy, Aarhus University, Spring 2026.

[2] A. Eidi, N. Zehtabiyan-Rezaie, R. Ghiassi, X. Yang, and M. Abkar, "Data-driven quantification of model-form uncertainty in Reynolds-averaged simulations of wind farms," *Physics of Fluids*, vol. 34, 085135, 2022.